(Received 5 April 2024, Accepted 31 May 2024, Scheduled 13 June 2024)

A Compact Two-Port Vivaldi-Based MIMO Antenna with High Isolation for C and X Bands Applications

Rong Li[1], Haoyu Zhang[1], Yanhong Xu[1,*], and Jianqiang Hou[2]

[1]*Xi'an Key Laboratory of Network Convergence Communication, College of Communication and Information Engineering Xi'an University of Science and Technology, Xi'an 710054, China*
[2]*National Key Laboratory of Science and Technology on Antenna and Microwave, Xidian University, Xi'an 710071, China*

ABSTRACT: This paper presents a broadband high-isolated MIMO antenna operating in the C and X bands simultaneously. The antenna is expected to be applied in wireless systems such as satellites and radar. A modified Vivaldi element is firstly designed by etching a rectangular structure out of the top metal, and then arranged symmetrically to form a 2-element broadband MIMO antenna with element spacing of 0.28λ (λ is the wavelength at 9 GHz). The operating frequency the MIMO antenna in terms of $S_{11} \leq -9.0$ dB is from 4.0 GHz to 13.5 GHz. However, the mutual coupling between the two elements is quite strong, which can be as high as 8.0 dB, indicating a severe mutual coupling effect between the elements. To improve the isolation level, a defect-ground structure (DGS) is designed and loaded on the ground plane. The decoupling structure of the DGS achieves decoupling in the C and X bands, with a particular emphasis on decoupling in the C band by blocking the current flow between antenna elements. The simulated result shows that the S_{21} can be lowered to less than -23.4 dB across the whole operating frequency region, i.e., an isolation improvement of 15 dB is achieved. A prototype is fabricated and measured. The measured results are in good agreement with the simulated ones, indicating that the designed broadband MIMO antenna is a good candidate for reliable communication in the C and X bands.

1. INTRODUCTION

Broadband technology is a carrierless communication technology characterized by high transmission rate, high processing gain, and strong positioning capability [1, 2]. This technology was initially applied for military applications and has been utilized to develop radar devices with extremely high resolution. Although broadband communication technology is capable of enhancing the capacity for transmitting data, the amount of information it can accommodate is still limited. Multiple Input Multiple Output (MIMO) system is characterized by advantages such as high spectrum utilization, high channel reliability, and low error rates [3–5]. Among them, MIMO antennas, which are an important component of a MIMO system, are evolving towards broadband, miniaturization, low cost, and easy integration. In recent years, there has been an increasing trend in the integration level of electronic devices, leading to a continuous reduction in the physical space available for MIMO antennas. As a result, the mutual coupling between the antennas has significantly increased, severely impacting the information transmission between them. Enhancing the isolation between MIMO antennas can effectively improve the reliability of information transmission [6]. Therefore, decoupling of broadband MIMO antennas holds significant research significance.

The decoupling methods commonly employed in modern MIMO antenna systems include orthogonal decoupling, metasurface decoupling, the neutralization line method, and the defect ground method, among others. Orthogonal decoupling method is employed in [7] and [8] to achieve decoupling by placing antenna units orthogonal to each other, which improves the isolation between antennas. This method is simple but results in a larger space requirement for the system. In recent years, decoupling using metamaterials [9–11] has become popular. There are various structures of metamaterials, including electromagnetic bandgap (EBG) structures, complementary split-ring resonator (CSRR), and others. The decoupling structure, proposed in [9] as MTM-EMBG, achieves an isolation of 25 dB between array elements. The decoupling structure based on CSSR metamaterial, proposed in [10], enhances the isolation of the antenna array by 12 dB within the operating frequency range. High isolation levels can be achieved through the use of metamaterial decoupling methods, but the design process for metamaterial unit structures is complex. Refs. [12–18] respectively employ neutralization line and defect ground methods for decoupling, both of which act on the surface current of the antennas to achieve decoupling. In [12], a neutralization line is introduced between the antennas to provide an additional current path. By utilizing out-of-phase currents, the coupling between the antennas is reduced, ultimately achieving an isolation greater than 22 dB between the antennas. In [14], the isolation between antennas is improved by 8 dB compared to the predecoupling state by introducing T-shaped decoupling slots on the floor of the MIMO antenna. The isolation achieved is 16 dB. In [18], a three-level stepped slot is loaded on the ground plane between the antennas, effectively blocking the surface currents between adjacent antennas and achieving an isolation of 18 dB between the antennas.

* Corresponding author: Yanhong Xu (yanhongxuxidian@163.com).

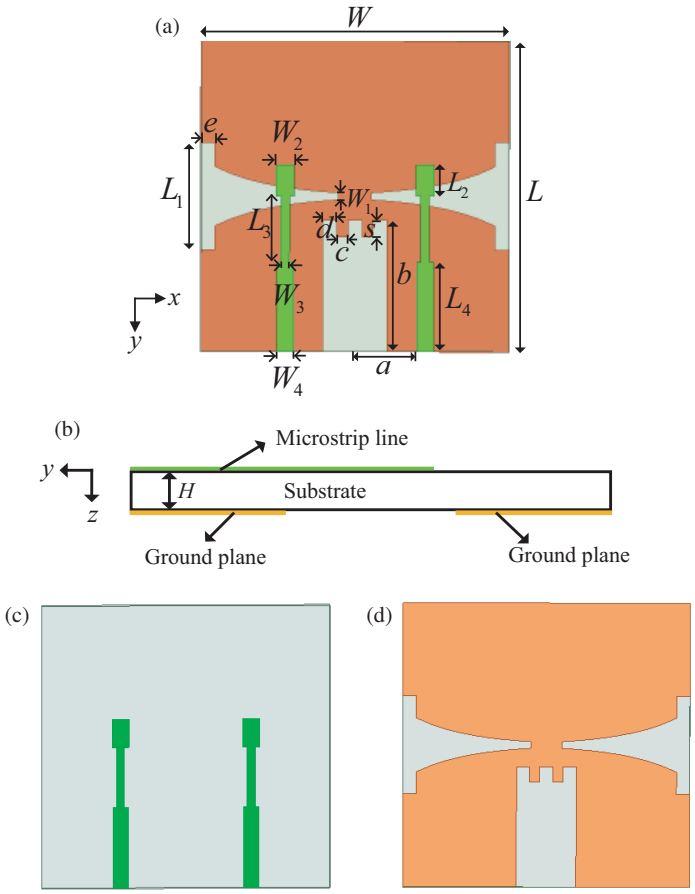

FIGURE 1. (a) The double-sided view. (b) Right side view. (c) Upper side view. (d) Lower side view (with $L = 26$, $L_1 = 9$, $L_2 = 2.6$, $L_3 = 5.5$, $L_4 = 7.5$, $W = 26$, $W_1 = 0.6$, $W_2 = 1.5$, $W_3 = 0.7$, $W_4 = 1.4$, $a = 4.7$, $b = 11$, $c = 0.9$, $d = 1.2$, $e = 1.2$, $s = 1.4$, $H = 0.762$ in mm).

To satisfy the demands of a larger channel capacity and higher data transmit rate, a two-port Vivaldi-based MIMO antenna with high isolation is designed which can operate in both the C and X bands simultaneously. The frequency region of the C band is from 4 GHz to 8 GHz, and the counterpart of the X band is from 8 GHz to 12 GHz. Besides, the designed MIMO antenna is compact in size, with overall dimensions of $26 \times 26 \times 0.762\,\text{mm}^3$, which can save space for other components in wireless communication systems such as radar and satellite. By incorporating the decoupling structure without altering individual Vivaldi elements, the antenna achieves a high isolation level of over 23.4 dB across the entire operating frequency range. The antenna designed in this paper possesses advantages of such as small size, high isolation, low envelope correlation coefficient, and simple decoupling structure.

2. ANTENNA DESIGN

2.1. Structure of the Proposed MIMO Antenna

The two sides of the antenna are shown in Figure 1(a), and Figure 1(b) depicts the right view of the antenna. Figures 1(c) and (d) present the upper and lower side views of the dielectric substrate. From Figure 1, it can be observed that the antenna is composed of a microstrip line, a ground plane, and a dielectric substrate. The material of the dielectric substrate is Taconic RF-30, with a relative permittivity of 3 and a loss tangent of 0.0014. The thickness of the substrate is 0.762 mm. The decoupling structure is slotted in the ground plane to achieve high isolation between antenna units.

2.2. Design of MIMO Antenna with High Isolation

The simulation of antenna is based on HFSS 2021R1 version. The design process of the antenna, as shown in Figure 2(a), is divided into four steps: Firstly, the tapered slot antenna is designed based on curve function Eq. (1). Secondly, rectangular slots are added to widen the wide slot line of the tapered slot. According to the characteristics of the Vivaldi antenna, the width of the slot line affects the position of the antenna's low-frequency point. Therefore, the purpose of adding rectangular slots is to widen the width of the slot line, causing the low-frequency point to shift to the left and thus broaden the antenna bandwidth. Thirdly, the antennas are symmetrically arranged to form a broadband MIMO antenna. Finally, a decoupling structure is loaded on the ground plane of the antenna to obtain a broadband and high-isolation MIMO antenna. The current at the excitation port of the antenna unit couples to the unexcited port, causing mutual coupling between the antennas. By loading a defective ground structure between the antenna units, the purpose of blocking the flow of current between the antennas

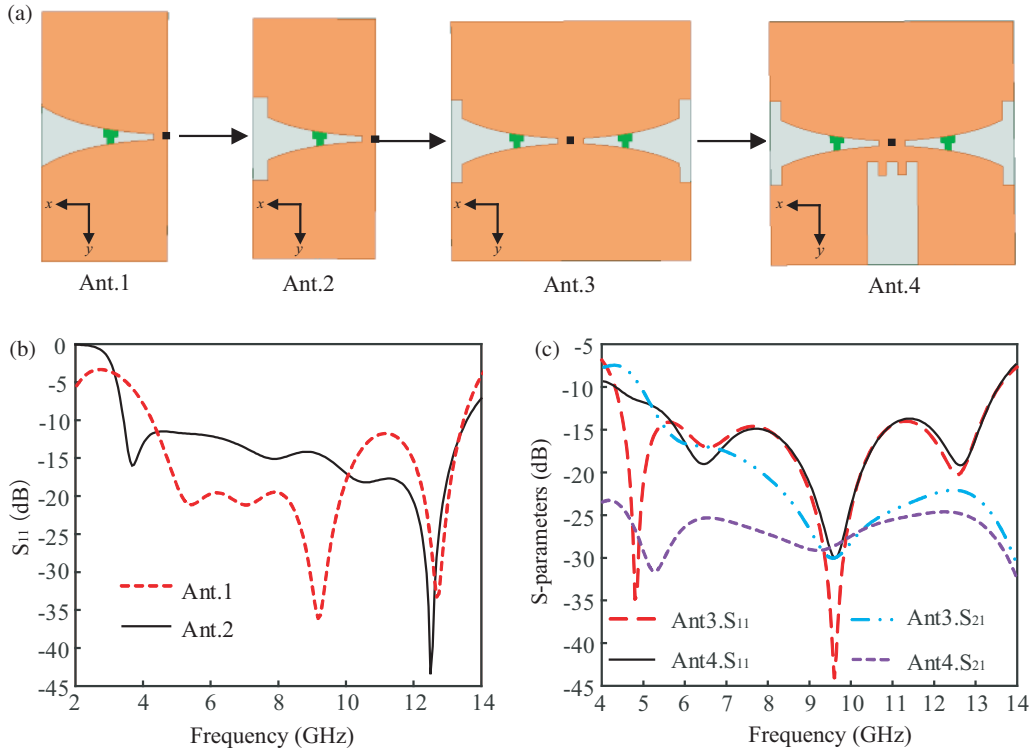

FIGURE 2. (a) Design procedures of the antenna. (b) S_{11} parameter curves for antennas 1 and 2. (c) S-parameter curves for antennas 3 and 4.

can be achieved. This helps in concentrating the current mainly on the slotted part of the decoupling structure, thereby improving the isolation between the antennas. The tapered curve function of the Vivaldi antenna is depicted as follows:

$$y = c_1 e^{Rx} + c_2 \tag{1}$$

The constants c_1 and c_2 are primarily influenced by the starting positions $P_1(x_1, y_1)$, and $P_2(x_2, y_2)$ of the slot lines. The expressions for these constants are as follows:

$$c_1 = \frac{y_2 - y_1}{e^{Rx_2} - e^{Rx_1}} \tag{2}$$

$$c_2 = \frac{y_1 e^{Rx_2} - y_2 e^{Rx_1}}{e^{Rx_2} - e^{Rx_1}} \tag{3}$$

The starting position of the exponential curve in this paper, P_1 (1.4, 0.3), and the ending position, P_2 (13, 3.15), are considered. The curvature R is equal to 0.2. Substituting these values into Eqs. (2) and (3) yields the constants $c_1 = 0.235$ and $c_2 = -0.01$.

Figure 2(b) displays the S_{11} plots of antenna 1 and antenna 2, with antenna 1 exhibiting a bandwidth of 4.5 to 13.5 GHz. Antenna 2 is obtained by widening the width of the long slot in antenna 1 through the addition of a rectangular groove. The bandwidth of antenna 2 is 3.51∼13.5 GHz, which allows the complete coverage of C and X bands, enabling communication between the C and X bands. The S-parameter plots for antennas 3 and 4 are shown in Figure 2(c), and the working frequency range of both antennas is 4∼13.5 GHz. The isolation between antenna 3 elements is measured to be 8 dB, indicating a significant mutual coupling effect between the antennas. After the decoupling structure is integrated, an isolation of greater than 23.4 dB is achieved by antenna 4 across the entire operating frequency range.

Parameters b and s are both related parameters of the decoupling structure. The shape and size of the decoupling structure defects have a crucial impact on the decoupling effect between antennas. Under the premise of scanning all parameters of the decoupling structure, S-parameter analysis graphs for parameters b and s are provided. The impact of different parameters b on the antenna's S_{21} is shown in Figure 3(a). From the figure, it can be observed that as parameter b increases, the isolation between the antennas becomes higher in the low-frequency range, indicating that the longer side of the defect structure functions as a barrier to current flow at lower frequencies. When parameter b is set to 11 mm, the isolation between antenna elements is maximized throughout the entire operating frequency range. Therefore, parameter b for the long side of the decoupling structure is chosen as 11 mm. The effect of parameter s on S_{21} is shown in Figure 3(b). It can be observed that parameter s primarily influences the decoupling performance at high frequencies. When s is set to 1.4 mm, the best decoupling effect at high frequencies is achieved.

The surface current distributions of antennas 3 and 4 at 5 GHz, 9 GHz, and 13 GHz are shown in Figure 4. From the figure, it can be observed that the decoupling structure reduces the influence of the excitation antenna unit's surface current on the unexcited unit. By slotting on the metal ground plane, the surface current paths between antenna units can be effectively altered. This causes the surface current to mainly concentrate around the defect structure. The current generated at the excita-

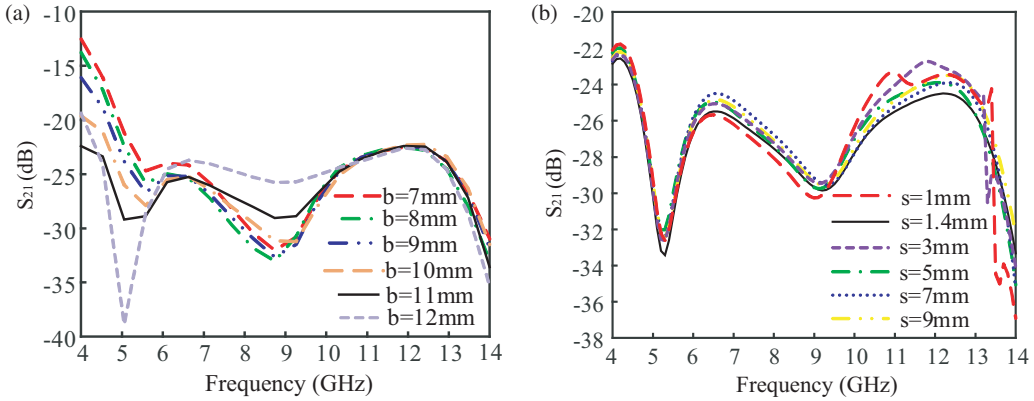

FIGURE 3. Simulated S_{21} with respect to (a) b, (b) s.

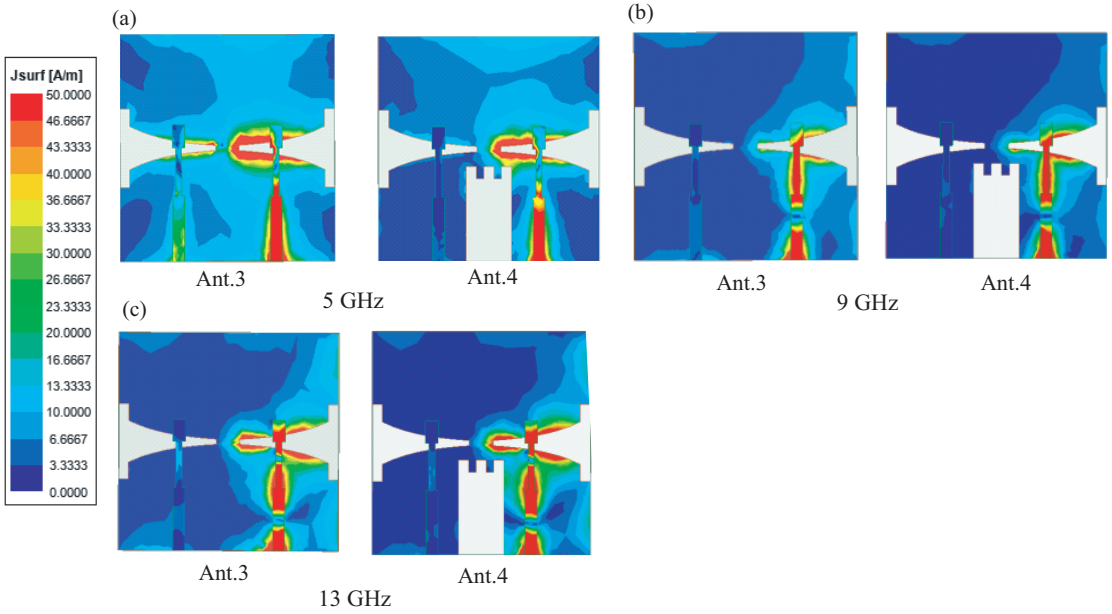

FIGURE 4. Simulated current distributions of the MIMO antenna at 5, 9, and 13 GHz during decoupling stages.

tion port is blocked by the defect structure, which effectively increases the effective distance between the antennas. Ultimately, this achieves the goal of increasing the isolation between the antennas. The decoupling structure primarily targets decoupling in the low-frequency range, which is consistent with the trend of S_{21} for antennas 3 and 4.

During the research on decoupling Vivaldi antennas, some scholars have proposed using T-shaped slots between the antennas for decoupling. However, this type of T-shaped slot can only improve the isolation between the antennas to 17 dB, which is relatively lower than the improvement in isolation achieved by this design. The corresponding descriptions have been added in the revised manuscript.

3. SIMULATED AND MEASURED RESULTS

To validate our work, a prototype of the proposed antenna is provided in Figure 5(a). The prototype of the proposed MIMO antenna is measured in the anechoic chamber. During the measurement, the prototype is placed on a turntable, and a standard horn antenna, termed horn 1, is utilized as the receiver at the same horizontal level in the far-field region of the prototype. The measured results are acquired by applying an Agilent N5244A network analyzer. The environmental image of the antenna in the microwave anechoic chamber is shown in Figure 5(b).

The correlation S-parameter plot of antenna 4 is shown in Figure 5(c), revealing that the operating frequency range of antenna 4 is from 4 to 13.5 GHz. The isolation between the elements of antenna 4 is greater than 23.4 dB, representing an improvement of more than 15 dB compared to the pre-decoupling antenna isolation. The simulated and measured results of the antenna are in good agreement. The gain and ECC (envelope correlation coefficient) plots of the antenna are shown in Figure 5(d). When measuring the antenna gain, another standard horn antenna, termed horn 2, is fabricated on the turntable in lieu of the prototype. The signal transmitted by the prototype and received by horn 1 is compared with the signal transmitted

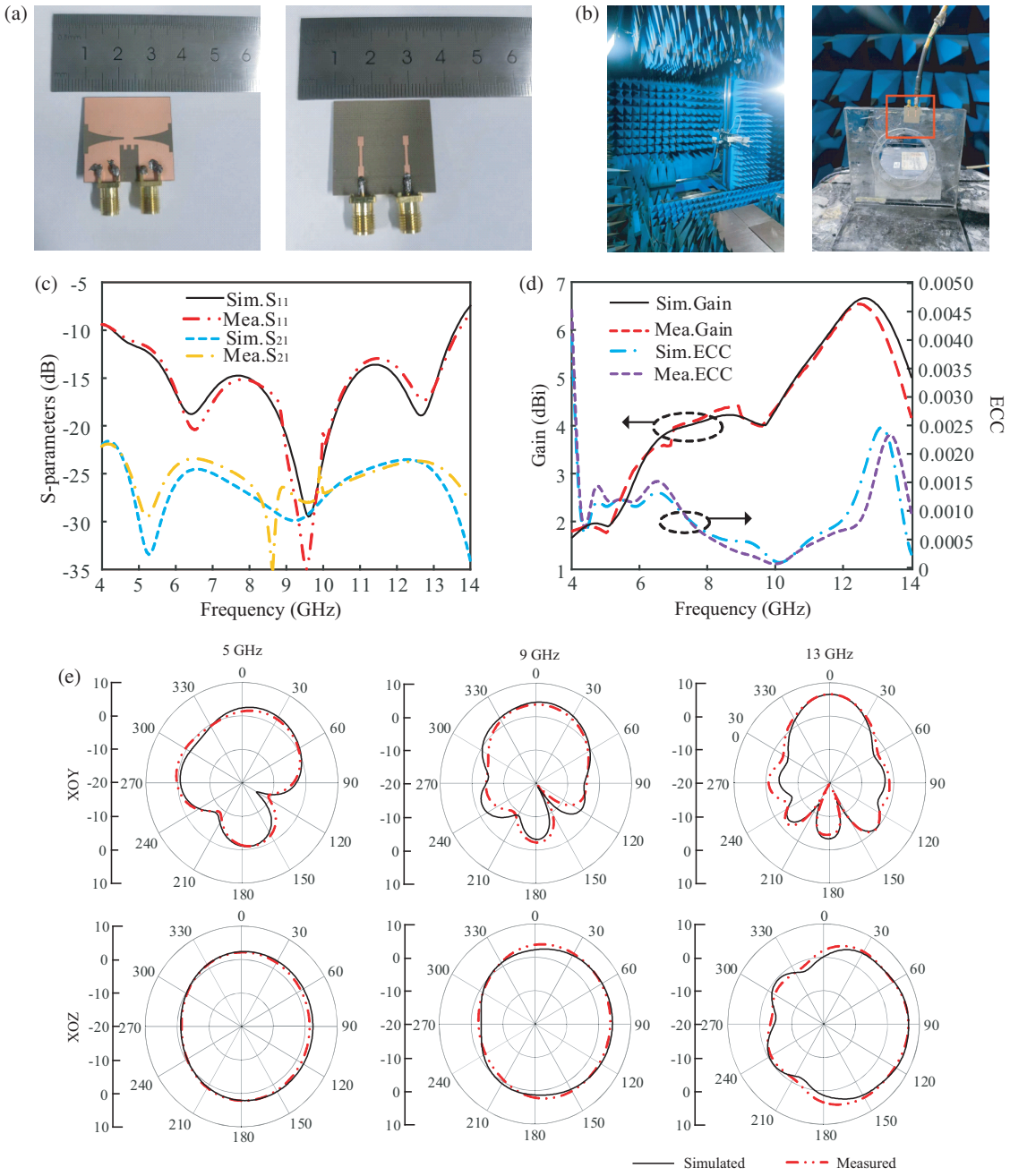

FIGURE 5. (a) Simulated antenna corresponding prototype. (b) Physical antenna test environment. (c) Simulated and measured S-parameter. (d) Simulated and measured gains and ECCs. (e) Simulated and measured radiation patterns.

by horn 2 and received by horn 1. In this way, the gain of the prototype is obtained since the gain of horn 2 is known. From the figure, it can be observed that the gain range of antenna 4 is $1.8 \sim 6.7$ dBi. The ECC is an important parameter for evaluating the diversity performance of MIMO systems. Assuming a uniform distributed flat fading multipath transmission for the antenna propagation path, the ECC can be obtained through Eq. (4). From the figure, it can be observed that the envelope correlation coefficient between the antennas is less than 0.0045 across the entire frequency range and even lower than 0.002 within the operating frequency range. Compared with the requirement of ECC below 0.5, it can be said that the correlation between the antennas is very low, indicating that the antenna designed in this paper exhibits excellent MIMO diversity performance. The simulated and measured curves in the figure match well.

$$ECC = \frac{\left| \iint\limits_{4\pi} \left[\overset{r}{E}_i(\theta,\phi) \cdot \overset{r}{E}_j^*(\theta,\phi) \right] d\Omega \right|^2}{\iint\limits_{4\pi} \left| \overset{r}{E}_i(\theta,\phi) \right|^2 d\Omega \iint\limits_{4\pi} \left| \overset{r}{E}_j(\theta,\phi) \right|^2 d\Omega} \tag{4}$$

TABLE 1. Performance comparisons of the MIMO antennas.

Reference	Size (mm^3)	Space (λ)	Gain (dBi)	Bandwidth (GHz)	Isolation (dB)	ECC
[14]	$26 \times 26 \times 0.762$	0.32	$0 \sim 5$	$2.9 \sim 11.6$	≥ 16	≤ 0.02
[17]	$26 \times 24.5 \times 0.6$	0.28	$0 \sim 5$	$2.5 \sim 12.0$	≥ 15	≤ 0.02
[19]	$42 \times 25 \times 1.6$	0.31	$0 \sim 7$	$3.2 \sim 12$	≥ 22	≤ 0.004
[20]	$25 \times 39 \times 0.8$	0.42	$2 \sim 5.2$	$2.68 \sim 12.5$	≥ 20	≤ 0.01
This work	$26 \times 26 \times 0.762$	0.28	$1.8 \sim 6.7$	$4 \sim 13.5$	≥ 23.4	≤ 0.002

Figure 5(e) shows the simulated and measured radiation patterns of antenna 4 at the frequency points of 5 GHz, 9 GHz, and 13 GHz. During the measurement, the standard horn antenna is fixed in the same position while the prototype rotates with the turntable in a horizontal plane. It should be highlighted that the prototype is placed horizontally and vertically on the turntable respectively for the measurement of patterns in the XOY and XOZ planes. From the figure, it can be observed that there is good consistency between the measured and simulated radiation patterns of the antenna. Additionally, as the frequency increases, the antenna exhibits stronger directivity.

A comparison is made between the performance of the broadband high-isolation MIMO antenna designed in this paper and antennas designed by other researchers. The results are shown in Table 1. The broadband antennas in [14] and [17] have a wider bandwidth than the antenna designed in this paper. However, they have lower gain and lower isolation between the antennas. The isolation in [19] and [20] exceeds 20 dB, indicating a higher separation between the antenna elements. However, the overall size of the antennas in those papers is larger than the antenna designed in this study. Taking into account the parameters in Table 1, the antenna designed in this paper is characterized by its small size, high isolation, low envelope correlation coefficient, and excellent MIMO diversity performance. These characteristics attest to the superior performance of the antenna, ensuring reliable data transmission during antenna communication.

4. CONCLUSION

A dual-element Vivaldi broadband high-isolation MIMO antenna operating in the C and X bands is designed in this paper. This antenna holds potential for applications in communication systems such as satellites and radar. Firstly, the original bandwidth of the Vivaldi antenna is $4.5 \sim 13.5$ GHz. By adding rectangular slots, the operating frequency range of the antenna is extended to $3.5 \sim 13.5$ GHz. Next, the antennas are symmetrically placed with a spacing of 0.28λ between the antenna ports. At this point, the isolation between the antennas is measured at 8 dB, indicating severe mutual coupling between the antennas. Finally, a decoupling structure of DGS is incorporated. The operating frequency of the MIMO antenna in terms of $S_{11} \leq -9$ dB is from 4 GHz to 13.5 GHz. Compared to the isolation before decoupling, the isolation has been increased by 15 dB, indicating that the antenna elements can operate independently without interfering with each other. The designed broadband high-isolation MIMO antenna overcomes the issue of severe mutual coupling between antennas, resolving the problem of interference among MIMO antennas during information transmission. However, since the decoupling structure in this paper primarily targets decoupling in the low-frequency range between antennas, it is possible to further enhance isolation in the high-frequency range by incorporating additional decoupling methods in the future. By combining different decoupling techniques, the overall isolation between the antennas can be comprehensively improved.

ACKNOWLEDGEMENT

This work was supported in part by the National Natural Science Foundation of China under Grant No. 62271386 and No. 61901357, and in part by the Shaanxi Provincial Association for Science and Technology Young Talents Trusteeship Program, grant 20230149.

REFERENCES

[1] Cicchetti, R., E. Miozzi, and O. Testa, "Wideband and UWB antennas for wireless applications: A comprehensive review," *International Journal of Antennas and Propagation*, Vol. 2017, Article ID 2390808, 2017.

[2] Rao, G. S., S. S. Kumar, and R. Pillalamarri, "Analysis and review on usage of broadband techniques in design of printed antennas for UWB communications," *Microsystem Technologies*, Vol. 21, 1423–1426, 2015.

[3] Zhang, Y.-M., S. Zhang, J.-L. Li, and G. F. Pedersen, "A transmission-line-based decoupling method for MIMO antenna arrays," *IEEE Transactions on Antennas and Propagation*, Vol. 67, No. 5, 3117–3131, 2019.

[4] Liu, L., S. Tian, D. Xue, T. Zhang, Y. Q. Chen, and S. Zhang, "A review of industrial MIMO decoupling control," *International Journal of Control, Automation and Systems*, Vol. 17, No. 5, 1246–1254, 2019.

[5] Varzakas, P., "Average channel capacity for Rayleigh fading spread spectrum MIMO systems," *International Journal of Communication Systems*, Vol. 19, No. 10, 1081–1087, 2006.

[6] Janaswamy, R., "Effect of element mutual coupling on the capacity of fixed length linear arrays," *IEEE Antennas and Wireless Propagation Letters*, Vol. 1, 157–160, 2002.

[7] Deshpande, R. and Y. U. Devi, "Hexa-slot wheel shaped fractal orthogonal MIMO antenna with polarization diversity for UWB applications," *Progress In Electromagnetics Research Letters*, Vol. 116, 31–38, 2024.

[8] Sehgal, P. and K. Patel, "Triband dual port h-SRR MIMO antenna for WLAN/WiMAX/Wi-Fi 6 applications," *Progress In*

Electromagnetics Research M, Vol. 123, 35–43, 2024.

[9] Alibakhshikenari, M., M. Khalily, B. S. Virdee, C. H. See, R. A. Abd-Alhameed, and E. Limiti, "Mutual-coupling isolation using embedded metamaterial EM bandgap decoupling slab for densely packed array antennas," *IEEE Access*, Vol. 7, 51 827–51 840, 2019.

[10] Wang, Z., C. Li, and Y. Yin, "A meta-surface antenna array decoupling (MAAD) design to improve the isolation performance in a MIMO system," *IEEE Access*, Vol. 8, 61 797–61 805, 2020.

[11] Hsu, C.-C., K.-H. Lin, and H.-L. Su, "Implementation of broadband isolator using metamaterial-inspired resonators and a T-shaped branch for MIMO antennas," *IEEE Transactions on Antennas and Propagation*, Vol. 59, No. 10, 3936–3939, 2011.

[12] Zhang, S. and G. F. Pedersen, "Mutual coupling reduction for UWB MIMO antennas with a wideband neutralization line," *IEEE Antennas and Wireless Propagation Letters*, Vol. 15, 166–169, 2015.

[13] Dkiouak, A., M. E. Ouahabi, S. Chakkor, M. Baghouri, A. Zakriti, and Y. Lagmich, "High performance UWB MIMO antenna by using neutralization line technique," *Progress In Electromagnetics Research C*, Vol. 131, 185–195, 2023.

[14] Li, Z., C. Yin, and X. Zhu, "Compact UWB MIMO Vivaldi antenna with dual band-notched characteristics," *IEEE Access*, Vol. 7, 38 696–38 701, 2019.

[15] Sharawi, M. S., M. Ikram, and A. Shamim, "A two concentric slot loop based connected array MIMO antenna system for 4G/5G terminals," *IEEE Transactions on Antennas and Propagation*, Vol. 65, No. 12, 6679–6686, 2017.

[16] Madhav, B. T. P., Y. U. Devi, and T. Anilkumar, "Defected ground structured compact MIMO antenna with low mutual coupling for automotive communications," *Microwave and Optical Technology Letters*, Vol. 61, No. 3, 794–800, 2019.

[17] Li, D.-H., F.-S. Zhang, G.-J. Xie, H. Zhang, and Y. Zhao, "Design of a miniaturized UWB MIMO Vivaldi antenna with dual band-rejected performance," *IEICE Electronics Express*, Vol. 17, No. 16, 20 200 233–20 200 233, 2020.

[18] Huang, H.-F. and S.-G. Xiao, "Compact UWB MIMO ground linearly tapered slot antenna decoupled by a stepped slot," *Progress In Electromagnetics Research C*, Vol. 71, 17–23, 2017.

[19] Srivastava, G. and A. Mohan, "Compact MIMO slot antenna for UWB applications," *IEEE Antennas and Wireless Propagation Letters*, Vol. 15, 1057–1060, 2015.

[20] Tang, Z., J. Zhan, X. Wu, Z. Xi, L. Chen, and S. Hu, "Design of a compact UWB-MIMO antenna with high isolation and dual band-notched characteristics," *Journal of Electromagnetic Waves and Applications*, Vol. 34, No. 4, 500–513, 2020.